VIP *Very Important Paper*

Palladium-Based Bimetallic Nanocrystal Catalysts for the Direct Synthesis of Hydrogen Peroxide

Sheng Wang,[a, b] Dmitry E. Doronkin,[a, c] Martin Hähsler,[a, b] Xiaohui Huang,[d] Di Wang,[d, e] Jan-Dierk Grunwaldt,[a, c] and Silke Behrens*[a, b]

The direct synthesis of H_2O_2 from H_2 and O_2 is a strongly desired reaction for green processes and a promising alternative to the commercialized anthraquinone process. The design of efficient catalysts with high activity and H_2O_2 selectivity is highly desirable and yet challenging. Metal dopants enhance the performance of the active phase by increasing reaction rates, stability, and/or selectivity. The identification of efficient dopants relies mostly on catalysts prepared with a random and non-uniform deposition of active and promoter phases. To study the promotional effects of metal doping on Pd catalysts, we employ colloidal, bimetallic nanocrystals (NCs) to produce catalysts in which the active and doping metals are colocalized to a fine extent. In the absence of any acid and halide promotors, PdSn and PdGa NCs supported on acid-pretreated TiO_2 (PdSn/s-TiO_2, PdGa/s-TiO_2) were highly efficient and outperformed the monometallic Pd catalyst (Pd/s-TiO_2), whereas in the presence of an acid promotor, the overall H_2O_2 productivity was also further enhanced for the Ni-, Ga-, In-, and Sn-doped catalysts with respect to Pd/s-TiO_2.

Introduction

Hydrogen peroxide is used industrially as bleaching agent in the pulp and paper industry, in chemical manufacture (e.g., to replace Cl-containing oxidants), and as a disinfectant.[1] As a green and selective oxidant, H_2O_2 has been applied in various oxidation reactions (e.g., olefin epoxidation).[1,2] The global H_2O_2 market demand was 3850 kt in 2015 and is expected to reach approximately 6000 kt in 2024.[3] On an industrial scale, H_2O_2 is manufactured mainly by the Riedl–Pfleiderer process, which involves the cyclic auto-oxidation of anthraquinones.[1] This process requires large-scale infrastructure and produces highly concentrated H_2O_2 (up to 70 wt% H_2O_2), however, for many applications only dilute H_2O_2 solutions ($<$9 wt%) are needed.[4] The Riedl–Pfleiderer process is considered to be non-green for a number of reasons and has significant capital expenditures and operating costs. Its deficiencies have motivated academia and industry to develop alternative processes for H_2O_2 synthesis, in particular its direct synthesis from O_2 and H_2 and electrochemical methods, which share similar attributes in terms of catalysis.[4]

Electrochemical H_2O_2 production proceeds by the cathodic two-electron reduction of O_2 with noble metals and their alloys (e.g., Pd-Au,[5] Pd-Hg,[6] Pt-Hg)[7] or metal-free, carbon-based materials[3,8] as electrocatalysts. Recently, the direct electrosynthesis of pure aqueous H_2O_2 solution (up to 20 wt%) was achieved in combination with a solid electrolyte.[9] The photocatalytic production of H_2O_2 from O_2 and H_2O using solar energy is highly interesting, for example, for use as a sustainable solar fuel in personal-based electrical items (e.g., in one-compartment H_2O_2 fuel cells).[8c,10] However, the low photocatalytic efficiency is still a big challenge.[11]

The direct synthesis of H_2O_2 from molecular H_2 and O_2 is another green and economically viable alternative for H_2O_2 production with clear benefits over the Riedl–Pfleiderer process as the infrastructure is simplified, less energy is consumed, green

[a] Dr. S. Wang, Dr. D. E. Doronkin, M. Hähsler, Prof. J.-D. Grunwaldt, Dr. S. Behrens
Institute of Catalysis Research and Technology
Karlsruhe Institute of Technology
Hermann-von-Helmholtz-Platz 1,
76344 Eggenstein-Leopoldshafen (Germany)
E-mail: silke.behrens@kit.edu

[b] Dr. S. Wang, M. Hähsler, Dr. S. Behrens
Institute of Inorganic Chemistry
Ruprecht-Karls University Heidelberg
Im Neuenheimer Feld 270, 69120 Heidelberg (Germany)

[c] Dr. D. E. Doronkin, Prof. J.-D. Grunwaldt
Institute for Chemical Technology and Polymer Chemistry
Karlsruhe Institute of Technology
Engesserstr. 20, 76131 Karlsruhe (Germany)

[d] X. Huang, Dr. D. Wang
Institute of Nanotechnology
Karlsruhe Institute of Technology
Hermann-von-Helmholtz-Platz 1,
76344 Eggenstein-Leopoldshafen (Germany)

[e] Dr. D. Wang
Karlsruhe Nano Micro Facility
Karlsruhe Institute of Technology
Hermann-von-Helmholtz-Platz 1,
76344 Eggenstein-Leopoldshafen (Germany)

Supporting Information and the ORCID identification number(s) for the author(s) of this article can be found under: https://doi.org/10.1002/cssc.202000407.

solvents (water or alcohols) are used, and organic substrates are absent.[2] Direct H_2O_2 synthesis can be implemented in decentralized plants of any size to enable the on-site production of H_2O_2 also on a small scale.[12] It has attracted great interest in academia and industry as such or in tandem with selective oxidation reactions (e.g., in the H_2O_2 to propylene oxide process[2] or in chemoenzymatic oxidation cascades).[13] Although the first patent for direct H_2O_2 synthesis was filed in 1914, its full industrial implementation has been hampered, primarily because of poor H_2O_2 selectivity.[14]

To date, most studies have been based on Pd nanoparticles, which remains the most active catalyst.[15] However, no Pd catalyst could meet the criteria for industrial H_2O_2 production as they also favor side reactions to H_2O, which reduces H_2O_2 selectivity. Acid (e.g., H_2SO_4) and/or halide (e.g., Cl^-, Br^-) promotors improve H_2O_2 selectivity by preventing the base-catalyzed decomposition of H_2O_2 and by blocking sites for further H_2O_2 conversion.[16] However, these liquid-phase promoters may lead to plant corrosion and leaching of the active metal particles and their effect on reactions that utilize H_2O_2 downstream is not well understood. Hence, the design of new catalysts with improved H_2O_2 selectivity and productivity in the absence of these promotors is very attractive but highly challenging. Various material properties have been identified experimentally that affect the overall performance of Pd catalysts in this reaction, which include particle size[17] and morphology,[18] surface adsorbates,[19] metal promotors, and the nature of the support.[20] To enhance H_2O_2 selectivity, recent studies have focused on the alloying of Pd and Pt with several transition metals (e.g., Au,[21] Ag[22]) and main group elements (e.g., Sn,[12] Sb,[23] Te[24]). In general, the enhanced catalytic properties of bimetallic catalysts have been attributed to synergistic effects and modified electronic and/or geometric surface structures of the active surface sites.[25] Heterogeneous catalysts produced by conventional impregnation and (co)precipitation procedures, however, are generally poorly defined because of the non-uniform particle size and random distribution of promotor and active phases, which make it difficult to attribute the catalytic properties to compositional changes. In this context, the "precursor concept" in which colloidal nanocrystals (NCs) are used as well-defined building blocks is a promising strategy to address the parameters that influence the catalyst performance. By this procedure, the NC composition is tuned independently, and active and doping phases are colocalized to a fine extent and preserved during the successive NC immobilization.

Herein, we report on a generalized procedure in which catalysts derived from bimetallic NCs were used to study the promotional effects of metal doping on Pd catalysts in direct H_2O_2 synthesis. This method relies on a single synthetic protocol, which provides us with a library of bimetallic PdM-based NCs with a tunable composition (M: Ni, Zn, Ga, In, Sn, Pb). The NCs were immobilized successively on an acid-pretreated TiO_2 support (s-TiO_2). Acid pretreatment was demonstrated previously to further enhance catalytic selectivity in direct H_2O_2 synthesis.[20b] We address the influence of metal doping and acid promotors in this reaction accordingly. The defined NC size and composition enables us to investigate structure–property relationships with the goal to identify true promotors in a systematic fashion. The catalytic performance of the NC-derived catalysts in direct H_2O_2 synthesis was investigated under environmentally benign and energy-economical reaction conditions (H_2, O_2 and N_2, 30 °C, ethanol) without the presence of any acid and halide promotors.

Results and Discussion

A library of different bimetallic PdM (M: Ni, Zn, Ga, In, Sn, Pb) NCs was prepared using a solution of the metal acetylacetonate (acac) or acetate (ac) precursor in oleyl amine (OLAM) and trioctyl phosphine (TOP). Typically, NCs are synthesized and stabilized in solution by the use of ligands, surfactants, or polymers. These organic molecules bind to the particle surface and further enhance the catalytic properties in direct H_2O_2 synthesis.[26] Therefore, to elucidate the specific effect of the metal dopants, organic ligands must be either removed by thermal or chemical treatment or the same type of ligand must be used for all of the NC-derived catalysts. Notably, thermal or chemical treatment may further affect the NC composition and lead to segregation, oxidation, or leaching selectively for one of the constituent elements. Our method relies on a single synthetic protocol with the same ligand composition to provide bimetallic PdM-based NCs with a tunable composition (M: Ni, Zn, Ga, In, Sn, Pb).

The same reaction conditions and a molar precursor ratio (Pd^{2+}/M^{n+}) of 2:1 were employed to synthesize all of the bimetallic NCs. In the case of Pd NCs, the reaction conditions were similar, but the reaction temperature did not exceed 200 °C. The stepwise increase of the reaction temperature from 60 to 200 and 300 °C led to the formation of well-defined bimetallic NCs. In the presence of TOP, pure Pd NCs nucleate at temperatures between 200 and 250 °C.[27] Previously, TOP was shown to displace acac from $Pd(acac)_2$ to form a stable $Pd^{II}(TOP)_4$ complex that may be further reduced by OLAM or excess phosphine.[27,28] OLAM was suggested to replace TOP in the Pd^{II} complex and to stabilize the final Pd^0 NCs.[27] Typically, bimetallic NCs are obtained at higher reaction temperatures (300 °C). Recently, it was suggested that Pd NCs form initially and control the decomposition of the second metal precursor that is then alloyed successively to yield the bimetallic PdM NCs.[29] The particle size and size distribution of the PdM NCs were determined by statistical measurement from a large number of NCs by using TEM (Figure 1 and Table 1). The mean particle size for Pd and PdM NCs was 3.5–6.7 nm (Figure S1 and Table S2). We used inductively coupled plasma optical emission spectroscopy (ICP-OES) to confirm the presence of both metals in the NCs (Table 1).

We analyzed the monometallic Pd and bimetallic PdM NCs by using XRD (Figure 2). The XRD patterns revealed very broad reflections of low intensity, which is characteristic for small NCs. For the majority of the NCs (i.e., PdNi, PdZn, PdGa, and PdIn), a single, broad reflection was observed at approximately $2\theta = 40°$, which is consistent with the (111) reflection of the monometallic NCs of the face-centered cubic (fcc) Pd phase.

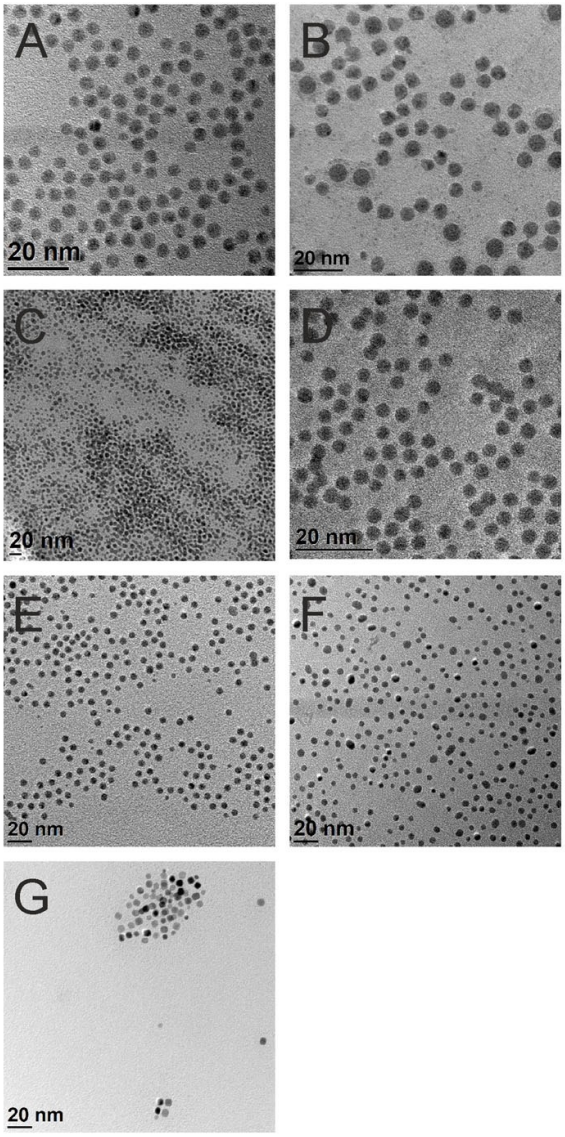

Figure 1. Representative TEM images of A) Pd NCs, B) PdNi NCs, C) PdZn NCs, D) PdGa NCs, E) PdIn NCs, F) PdSn NCs, and G) PdPb NCs.

The XRD patterns did not show any reflections characteristic of an ordered intermetallic phase, which suggests the random distribution of Pd and M (Ni, Zn, Ga, In) at fcc sites in these bimetallic NCs. For PdSn-based NCs the reflections were also broad and of low intensity but the diffraction pattern differed from that of the monometallic Pd reference particles (Figures S2 and S3).

Reflections could be assigned to the intermetallic Pd_2Sn phase (JCPDS 01-089-2057). The formation of Pd_2Sn NCs has been described previously by Luo et al.[30] For PdPb-based NCs, the diffraction pattern also differed from that of the fcc Pd phase of the monometallic Pd NCs; the reflections could be assigned mainly to intermetallic Pd_3Pb NCs (JCPDS00-050-1631) in the presence of some Pd NCs (Figure S3). As the overall molar Pd/Pb ratio was 2:1, this could point towards some surface segregation of Pb on the surface of the bimetallic particles.

Table 1. Metal loadings, NC sizes, and atomic compositions of the supported catalysts.

Supported catalyst	NC size[a] [nm]	Pd [wt%]	M [wt%]	Atomic NC comp.[a]
$Pd/s\text{-}TiO_2$	4.1 ± 1.6	5.6	–	Pd
$PdNi/s\text{-}TiO_2$	4.8 ± 1.6	2.5	0.5	$Pd_{0.74}Ni_{0.26}$
$PdZn/s\text{-}TiO_2$	5.7 ± 2.6	2.6	1.0	$Pd_{0.73}Zn_{0.27}$
$PdGa/s\text{-}TiO_2$	3.6 ± 1.9	2.6	0.6	$Pd_{0.76}Ga_{0.24}$
$PdIn/s\text{-}TiO_2$	3.6 ± 1.7	3.8	1.2	$Pd_{0.78}In_{0.22}$
$PdSn/s\text{-}TiO_2$	4.4 ± 2.0	4.1	2.8	$Pd_{0.62}Sn_{0.38}$
$PdPb/s\text{-}TiO_2$	4.8 ± 1.1	6.7	6.2	$Pd_{0.68}Pb_{0.32}$

[a] Mean diameters (and standard deviations) of the supported NCs were calculated from TEM images. [b] Total metal loadings of the supported catalysts and atomic compositions of the NCs were determined by using ICP-OES.

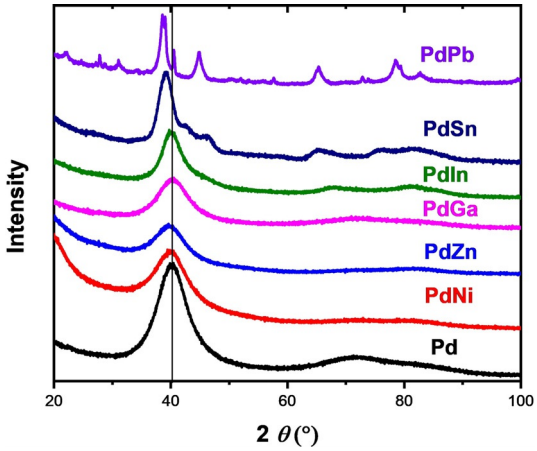

Figure 2. XRD patterns of Pd, PdNi, PdZn, PdGa, PdIn, PdSn, and PdPb NCs.

Reflections characteristic of the corresponding metal oxides were not observed by using XRD. However, we cannot exclude that a thin layer of metal oxide was formed after the NCs were exposed to air. Crystallite sizes of 2.2 (Pd NCs), 2.2 (PdNi NCs), 2.3 (PdZn NCs), 2.4 (PdGa NCs), and 3.7 nm (PdIn NCs) were calculated according to the Scherer equation, and the NC sizes were slightly larger for the PdSn NCs (6.5 nm) and PdPb NCs (6.0 nm) (Table S2).

A series of $PdM/s\text{-}TiO_2$ catalysts was prepared by the adsorption of the NCs from a colloidal solution in $CHCl_3$ onto the H_2SO_4-pretreated TiO_2 support. Previously, various materials have been employed to support the active metal phase in direct H_2O_2 synthesis (e.g., TiO_2,[20b,31] Al_2O_3,[32] SiO_2,[22,33] ZrO_2,[34] Fe_2O_3, zeolites,[35] heteropolyacids,[36] and carbon-based materials),[20b,21,37] and it is well known that the nature of the support has a significant effect on the catalyst activity and selectivity. A number of explanations have been proposed to account for the effect of the support, such as its acidity and isoelectric point, as a key factor for H_2O_2 stabilization or its influence on the electronic structure of the metal nanoparticles.[38] However, the support also controls the manner in which the active metal component is dispersed (in particular if prepared by conventional wet impregnation techniques) and a comparison between different types of support materials may be misleading. TiO_2 [P25, Evonik; anatase (80%)/rutile (20%), Brunauer–

Emmett–Teller (BET) surface area = 54 $m^2 g^{-1}$] is commercially available and was chosen in the present study as a benchmark support material for all NCs to compare the effect of metal doping on the catalytic properties of the Pd NCs. TiO_2 was shown to neither catalyze H_2O_2 hydrogenation nor its decomposition.[20b] TiO_2 was treated with H_2SO_4 before use, which was demonstrated previously to further enhance catalytic selectivity in direct H_2O_2 synthesis.[20a,b] From TEM images of the NCs immobilized on s-TiO_2, we can see that the NCs were well distributed over the s-TiO_2 support (Figure 3). After immobilization on the s-TiO_2 support, a relatively minor decrease in mean diameter was observed for most NCs (Figure S4 and Table S2). Although this decrease is not considered statistically relevant for the Pd, PdZn, and PdSn NCs, it is possible that the decrease in the size of PdIn, PdNi and PdPb NCs is caused by a restructuring of the NCs after immobilization. As such, the influence of NC restructuring on the catalytic performance cannot be completely excluded.

High-angle annular dark-field scanning transmission electron microscopy (HAADF-STEM) images of the supported catalysts with energy-dispersive X-ray (EDX) spectroscopy mapping of the NCs are shown in Figures S5 and S6.

The structure and composition of the s-TiO_2-supported NCs after pretreatment in H_2, similar to that employed during catalytic testing, were further investigated by using X-ray absorption spectroscopy (XAS). X-ray absorption near edge structure (XANES) spectra (Figure 4A) show only features attributed to metallic Pd (a double feature at ≈24360 and 24390 eV).[39] Notably, the spectral features are shifted in all XANES spectra of the bimetallic NCs compared to that the monometallic Pd NCs (to be able to see the difference, this spectrum is shown in gray and overlaid on each spectrum of the bimetallic NCs). Such shifts and differences in the near edge structure can be attributed to small differences in the electronic and/or geometric structure around the Pd atoms in the bimetallic NCs and, as in all cases the Pd surface was cleaned of adsorbed species by H_2, can only be attributed to the influence of the second metal. Hence, we used XANES to confirm the modification of the Pd lattice for all bimetallic NCs. Extended X-ray absorption fine structure (EXAFS) spectra (Figure 4B and Figure S8 for the raw data) are dominated by backscattering on Pd neighbors.[39] Hence, EXAFS spectra indicate the formation of metallic NCs

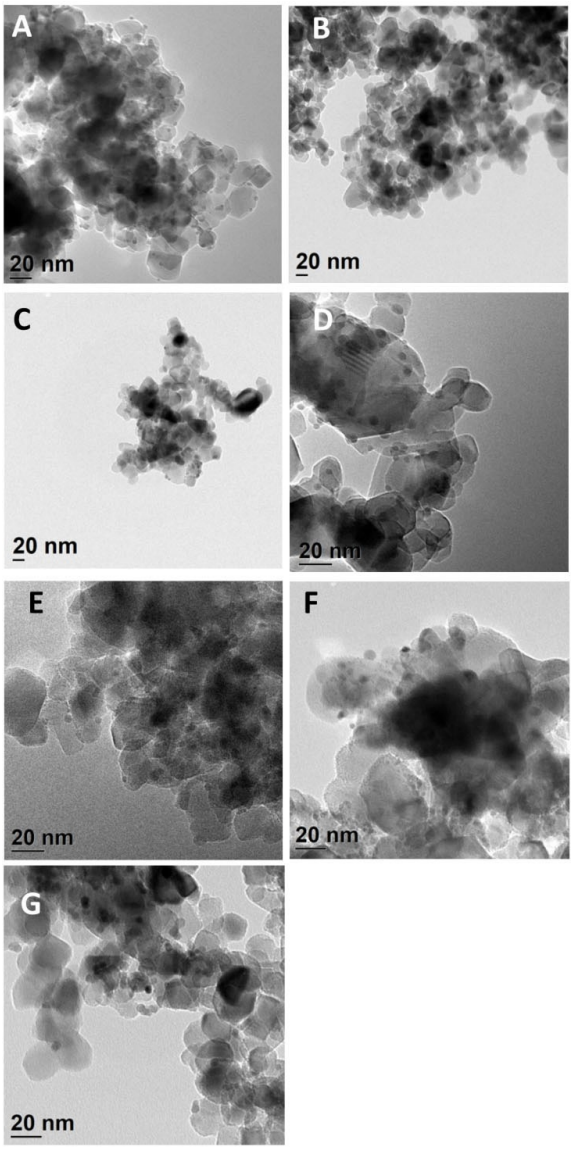

Figure 3. TEM images of NCs supported on s-TiO_2: A) Pd/s-TiO_2, B) PdNi/s-TiO_2, C) PdZn/s-TiO_2, D) PdGa/s-TiO_2, E) PdIn/s-TiO_2, F) PdSn/s-TiO_2, and G) PdPb/s-TiO_2.

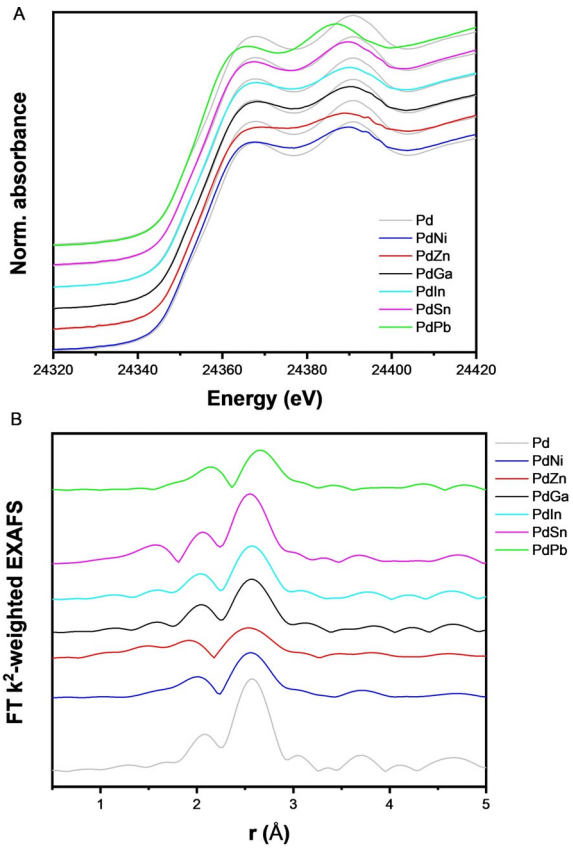

Figure 4. A) XANES and B) Fourier-transformed, k^2-weighted EXAFS spectra (uncorrected for the phase shift) of the bimetallic PdM/s-TiO_2 catalysts measured at the Pd K edge.

with a structure similar to monometallic Pd NCs, which is in good agreement with the results obtained by using XRD. Analysis of the EXAFS spectra (Table S3; EXAFS fits are reported in Figure S8) confirms the presence of Pd neighbors and, in some cases, second metal neighbors. Average Pd–Pd distances can be used to evaluate structure distortion in the metal NCs. As all NCs were of a similar size and measured under identical conditions, changes of the Pd–Pd distance relative to that in Pd metal and in pure Pd NCs could be attributed only to the doping of Pd NCs with a second metal or alloy formation. PdNi, PdZn, and PdPb NCs show statistically significant shifts of the average Pd–Pd distance to lower values. In the case of PdGa, PdNi, PdZn, and PdPb NC spectra, the EXAFS fits are considerably improved by also taking into account the second metal neighbors. Hence, the doping of Pd NCs by the second smaller metal possibly occurs in the PdGa, PdNi, and PdZn samples. The alloying of Pd with Pb resulted in the formation of a new structure, the EXAFS spectrum of which was best fitted by using the Pd_3Pb reference (space group $Pm\bar{3}m$; ICSD collection code 648357). The XANES spectrum of the PdPb sample at the Pb L_3 edge (Figure S7; H_2 treatment was not performed before this measurement) also revealed metallic features together with a strong shift of the absorption edge to higher energies, which indicates lower electronic density on Pb atoms because of alloy formation with Pd. For both PdSn and PdIn NCs, the Pd–Pd distances are similar to that in pure Pd and the second metal cannot be distinguished by using EXAFS analysis because the backscattering of Sn and In is very similar to that of Pd. Hence, in these two cases, only modification of the Pd electronic structure as seen by using XANES (Figure 4A) can confirm the doping of Pd by Sn and In. The alloying of Pd with Sn and In is further shown by using XRD and STEM-HAADF EDX, respectively.

There has been a great interest to enhance the catalytic performance and/or decrease the cost of noble-metal-based catalysts (Pd, Pt, Au) by introducing cost-effective, non-noble metal dopants (Table 2).[12,22,40] To understand the promotional effect of the different metal dopants, the catalytic performance of the supported NCs (PdM/s-TiO_2) was investigated by using a semicontinuous batch reactor with ethanol as a solvent in the presence and absence of H_2SO_4 as a promotor. The total metal content (Pd and M) was kept constant (i.e., 1.3 mg) for all catalytic experiments. Before catalytic testing, the suspended catalysts were activated in situ in H_2/N_2 atmosphere. PdO is already reduced under ambient conditions in H_2 atmosphere, whereas thin metal oxide surface layers formed by any of the dopant elements may not be reduced under these conditions.[39b] The catalytic performance of the NC-based catalysts is illustrated in Figure 5, which presents the concentration of H_2O_2 as function of the reaction time and productivity/selectivity/H_2 conversion, respectively. By doping the Pd NCs with Ga or Sn in PdGa/s-TiO_2 and PdSn/s-TiO_2, respectively, the concentration of H_2O_2 increased significantly with reaction time in the absence of an acid promotor, even though the Pd loading in the reactor was reduced

Table 2. Comparison of H_2O_2 selectivity and productivity for various bimetallic catalysts (for further details of catalyst testing see Table S7).

Reference	Catalyst[a]	Promotor	$S(H_2O_2)$ [%]	$P(H_2O_2)$ [mol kg_{Pd}^{-1} h^{-1}]
This work	Pd/s-TiO_2	–	21	1530
	PdGa/s-TiO_2	–	36	3610
	PdSn/s-TiO_2	–	51	4560
	Pd/s-TiO_2	H_2SO_4[b]	65	5420
	PdGa/s-TiO_2	H_2SO_4[b]	67	7480
	PdSn/s-TiO_2	H_2SO_4[b]	77	9240
Edwards[49]	Au(2.5)/Pd(2.5)/TiO_2	CO_2	70	2560
Solsona[32]	Au(2.5)/Pd(2.5)/Al_2O_3	CO_2	30	680
Freakley[12]	Pd(3)/Sn(2)/TiO_2	CO_2	96	2033
Tian[24]	Pd(3)Te(0.03)/TiO_2	H_2SO_4[b]	100	977
Han[33a]	Pd(3.3)Au(11.2)/SiO_2	HCl[b]	62	870
Bernardotto[34]	Pd(1.3)/Pt(0.2)/ZrO_2[f]	H_2SO_4[c]	56	1236
	Pd(1.3)Au(1.2)/ZrO_2[f]	H_2SO_4[c]	62	1190
Maity[43]	$Pd_{0.6}Ni_{0.4}$	HCl[d], Br[e]	82	1648
	$Pd_{0.6}Ni_{0.4}$	–	0	0
Wang[50]	Pd(1)Zn(5)/Al_2O_3	H_2SO_4[c]	79	25431

[a] The loading in wt% is given in brackets. Concentration of acid or halide promotors: [b] 0.12 M; [c] 0.03 M; [d] 0.1 M; [e] 0.01 M. [f] ZrO_2 was sulfated before use.

(Figure 5B). Bimetallic PdIn/s-TiO_2, PdNi/s-TiO_2, and PdZn/s-TiO_2 yielded a similar H_2O_2 concentration, and PdPb/s-TiO_2 produced less H_2O_2 over time than the Pd/s-TiO_2 reference, but the amount of Pd employed in these experiments was also lower. The doping of Pd NCs with either Ni or Ga in bimetallic PdNi/s-TiO_2 and PdGa/s-TiO_2 had a promotional effect on the H_2 conversion [$X(H_2)$] with an increase from 35 to 38 and 42%, respectively, whereas all other PdM NCs (In, Sn, Pb, and Zn) revealed lower H_2 conversions (Figure 6A). The segregation of some Pb on the surface of the bimetallic PdPb NCs may be the reason for the low H_2 conversion (12%) observed for these NCs. Ni is a well-known catalyst for hydrogenation reactions.[41] Although the presence of Ni enhanced the H_2 conversion over PdNi/s-TiO_2, a slightly decreased selectivity was observed (19%; Table S4).

The addition of Sn, Ga, or In promotors to Pd NCs yielded both significantly higher H_2O_2 selectivity (S) and productivity (P; PdSn/s-TiO_2: $S(H_2O_2) = 51\%$, $P(H_2O_2) = 4460$ mol kg_{Pd}^{-1} h^{-1};

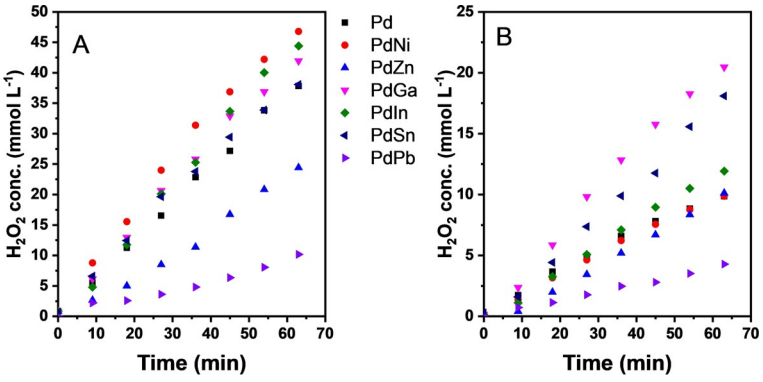

Figure 5. Concentration of H_2O_2 produced over bimetallic PdM/s-TiO_2 catalysts as a function of time: A) in the presence of H_2SO_4 promotor (0.12 M) and B) without H_2SO_4. The monometallic Pd/s-TiO_2 catalyst was used as a reference. Ethanol was employed as a solvent for catalytic testing.

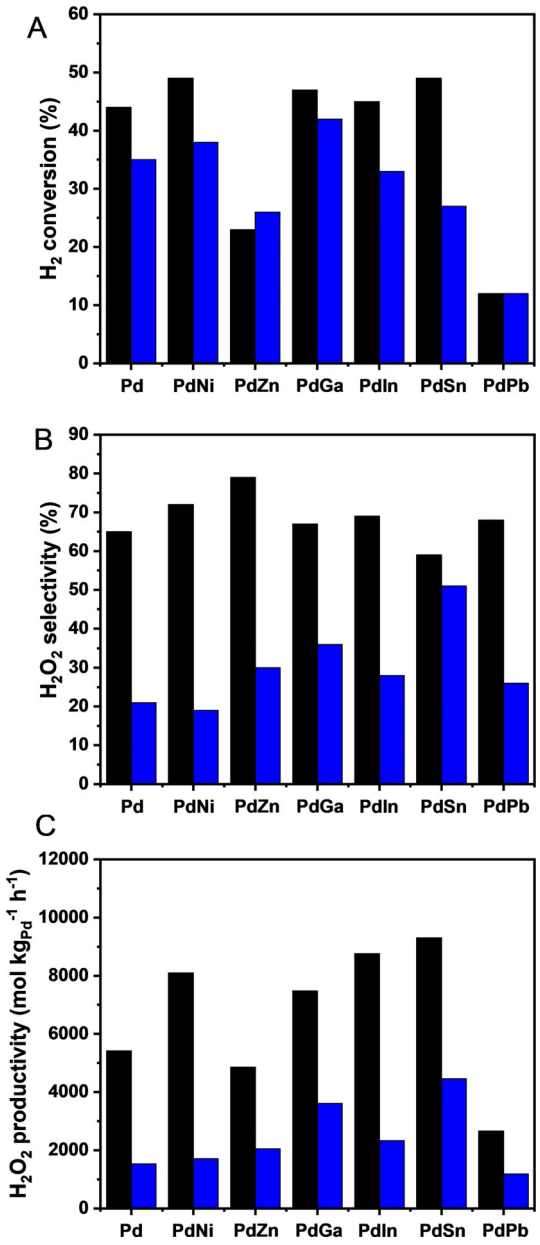

Figure 6. A) H_2 conversion, B) H_2O_2 selectivity, and C) H_2O_2 productivity [mol kg_{Pd}^{-1} h^{-1}] of the Pd/s-TiO_2 and PdM/s-TiO_2 catalysts in the direct synthesis of H_2O_2. Reaction medium: ethanol with H_2SO_4 promotor (black) and without any acid or halide promotor (blue).

PdGa/s-TiO_2: $S(H_2O_2) = 36\,\%$, $P(H_2O_2) = 3610$ mol kg_{Pd}^{-1} h^{-1}; PdIn/s-TiO_2: $S(H_2O_2) = 28\,\%$, $P(H_2O_2) = 2330$ mol kg_{Pd}^{-1} h^{-1}), whereas the H_2O_2 productivity was reduced after the alloying of Pd with Pb (Table S4). Previously, we showed that the introduction of small quantities of In and Ga, in particular, inhibit H_2O_2 degradation and enhance catalytic selectivity with respect to the analogous Pd catalyst.[42] Notably, In was leached during the catalytic reaction even in the absence of acid promotors and could not be recovered in the spent catalyst (Table S6). Overall, PdSn NCs were most efficient with a H_2O_2 productivity of 4460 mol kg_{Pd}^{-1} h^{-1} and 51 % H_2O_2 selectivity and clearly outperformed the monometallic Pd/s-TiO_2 reference catalyst in the absence of any halide or acid promotor (Figure 6C).

As expected, the addition of an acid promotor (H_2SO_4) led to an overall increase in H_2O_2 selectivity and production rate for all of the catalysts investigated in this study. Previously, it was reported that acid promotors prevent base-catalyzed H_2O_2 decomposition and stabilize the formed H_2O_2.[16a,21] Moreover, protons were suggested to be essential for H_2O_2 formation by a proton–electron transfer mechanism, whereas the nature and adsorption of the counter ions (SO_4^{2-}) on the active metal phase seemed to be less important.[15b] As expected, an increase in $X(H_2)$ and $S(H_2O_2)$ were observed for the monometallic Pd/s-TiO_2 catalyst (Table S5) in the presence of H_2SO_4 promotor. The H_2O_2 productivity of the Ni-, Ga-, In-, and Sn-doped catalysts was also further enhanced in the presence of H_2SO_4 promotor and superior to that of the monometallic Pd reference catalyst (Table S5). The enhancement of the productivity of Pd in the presence of Ni, for example, has been reported previously for direct H_2O_2 synthesis in the presence of promotors (HCl, Br^-), whereas no H_2O_2 formation occurred in the absence of promotors.[43] In other studies, the addition of Zn to Pd led to a 20- and 130-fold decrease in both H_2O_2 and H_2O formation rates, respectively, to result in an enhanced selectivity to H_2O_2 (69 %).[33b]

The addition of Zn was suggested to induce electronic changes of the active sites for O_2 reduction that favored H_2O_2 formation significantly, but the overall product turnover rate, mol(H_2O_2)/mol(metal surface atoms), was not further improved compared to that of the monometallic Pd catalyst. In the presence of an acid promotor, our Zn-doped NC catalyst revealed also an enhanced H_2O_2 selectivity (79 %), whereas both the H_2 conversion (23 %) and overall production rates (4860 mol kg_{Pd}^{-1} h^{-1}) remained low. Generally, however, the presence of an acid promotor led to severe catalyst leaching in our studies. Under these conditions, most of the dopants M could not be recovered in the spent catalysts, and soluble species may have contributed to these catalytic findings (Table S6). Some leaching may have also been caused by the detachment of whole NCs from the support (as also indicated by a loss of Pd metal) and attributed to the fact that our NC-based catalysts were not calcined before catalyst testing to preserve the size, shape, and composition of the original NCs in the supported catalysts. Only the intermetallic NCs PdSn and PdPb were relatively stable under acidic reaction conditions. Intermetallic NC compositions have not only been shown to have a tunable catalytic performance but also an enhanced catalyst stability.[44] Indeed, in the presence of an acid promotor, PdSn/s-TiO_2 was not only relatively stable but also showed the highest productivity (9200 mol kg_{Pd}^{-1} h^{-1}) of the NC-derived catalyst library (Tables S5 and S6).

In general, the enhanced H_2O_2 selectivity and productivity of multimetallic catalysts is attributed to various effects. Metal dopants (e.g., Au) were suggested to change the geometric surface structure to reduce the prevalence of multiple, contiguous Pd atoms on the catalyst surface,[5a] which in turn changes the distribution of active sites (i.e., ensemble effect) among those that preferentially form H_2O_2 (e.g., single Pd sites) and those that largely produce H_2O (e.g., groupings of multiple Pd atoms).[45] In other work, the increase in the Au/Pd

ratio in similarly sized Pd and Au_xPd_1 catalysts led to simultaneous but unequal increases in activation enthalpies for both H_2O_2 and H_2O formation, which were attributed to significant electronic changes of Pd by Au.[46] From DFT calculations and Sabatier analysis, the alloying of Pd with dopants of suitable electronegativity was suggested to adjust the valence electrons of Pd-shell atoms to an optimal range, which enhanced both the activity and selectivity in direct H_2O_2 synthesis.[47] From the catalytic results in this study, a simple correlation of the catalytic performance with the electronegativity of the employed metal dopants could not be derived. Previously, the high selectivity of Pd/Sn-based catalysts was suggested to originate from the encapsulation of small Pd-rich particles (size $\leq$2 nm) by a layer of SnO_x species after catalyst calcination, which suppressed H_2O_2 degradation on these surface sites rather than the formation of alloyed PdSn particles.[12] As we employed monodisperse PdSn NCs [mean size 4.8($\pm$0.8) nm] as precursors for catalyst preparation, a covering of ultra-small, nonselective Pd NCs did not seem to account for the increased H_2O_2 productivity here. In another study, the formation of SnO_x species was also observed on TiO_2-supported PdSn NCs under conditions of H_2O_2 synthesis.[31b] SnO_x was suggested to adsorb O_2 without O–O bond scission, and Pd(PdO) in close proximity to SnO_x was proposed to activate H_2, as H_2O_2 was generated rapidly at the Pd–SnO_x and PdO–SnO_x interface. An enhanced activity and selectivity and the role of Sn doping have also been reported for other types of hydrogenation reactions in which electronic effects (electron-donating effects from Sn to the noble metal) as well as the formation of SnO_2 close to the noble metal seemed to be responsible for the increased selectivity and activity.[48] Interface and electronic effects are often entangled and it is difficult to distinguish from each other. Thus, interface and electronic effects may also contribute to the enhanced H_2O_2 selectivity observed for other types of nonprecious metal dopants (e.g., Ga, In, Zn). This will be further addressed in future investigations.

An evaluation of the catalytic H_2O_2 selectivity and productivity is given in Table 2 (see Table S7 for full details of the reaction parameters). Previously, the modification of Pd by the addition of a range of precious or nonprecious metals has been demonstrated to enhance catalytic H_2O_2 selectivity and productivity. In accordance with these studies, we now report that the addition of Sn to our s-TiO_2-supported Pd NCs improves H_2O_2 selectivity and, importantly, leads to a significantly enhanced H_2O_2 productivity even in the absence of acid or halide promotors. The addition of acid promotors to the reaction medium may not only cause the leaching of the active phase but also reactor corrosion and necessitates additional purification steps, which make the above acid- and halide-free H_2O_2 synthesis in ethanol in the presence of Ga- and Sn-doped Pd catalysts highly attractive.[43] The alloying of precious-metal-based catalysts with low-cost and nontoxic metals is also an interesting approach towards economical and sustainable catalytic systems. The doping of Pd with nonprecious metals such as Ga or Sn lowers the metal cost of the catalyst by 7 and 33%, respectively, whereas the addition of Au increases them (e.g., by 19 and 62%, calculated for Pd/Au-based bimetallic catalysts reported in Refs. [20b and 33], respectively). Notably, the assessment of new catalyst compositions remains challenging, as catalytic selectivity and productivity are influenced not only by the catalyst material but also by the different parameters of catalyst testing (such as reactor type and details of reaction conditions; Table S7).[51] This further underlines the importance of well-defined model catalysts that enable the evaluation of metal dopant–performance relationships under comparable testing conditions.

Conclusions

We developed a library of monometallic Pd and bimetallic PdM (M = Ni, Zn, Ga, Sn, In, Pb) nanocrystals (NCs) using one synthetic protocol. A series of bimetallic NCs (i.e., PdNi, PdZn, PdGa, PdIn, PdSn, and PdPb) was obtained with sizes in the range of 3.5–6.7 nm and controlled compositions. The NCs were adsorbed successively from colloidal solution onto an acid-pretreated TiO_2 support. The catalytic performance was enhanced clearly in the presence of an acid promotor, and the doping of Pd NCs with Ni, Ga, In, and Sn further enhanced the H_2O_2 productivity. However, the presence of an acid promotor led to severe leaching and Ni, Ga, and In were not recovered from the spent catalyst. Only PdSn NCs were relatively stable under these reaction conditions. In pure ethanol and in the absence of additional halide or acid promotors, the PdGa and PdSn NC-derived catalysts were particularly promising and revealed an approximately 2.5–3-fold increase in H_2O_2 productivity compared to the Pd reference catalyst, respectively. In addition, Sn and Ga doping also significantly increased the selectivity from 21% (Pd-based reference) to 51 and 36%, respectively. The doping of Pd NCs with Ni, Zn, Ga, In, or Sn may not only influence the electronic and/or geometric surface structure of the NCs but also the formation of metal hydrides and oxides under the reaction conditions. In addition to the alloyed particle core, surface segregation of these dopants needs to be considered to lead to the formation of thin metal oxide surface layers under reaction conditions and probably contributes to the overall catalytic behavior. In general, the interplay of the different materials parameters is rather complex and, so far, there seems to be no simple materials descriptor. Therefore, insights into the structural evolution of these different and defined catalysts under the working conditions will be particularly attractive in future investigations and may contribute to the further understanding of the influence of the individual material parameters on the overall catalytic behavior.

Experimental Section

Nanocrystal synthesis: All procedures for NC synthesis were performed using standard Schlenk techniques. In a typical NC synthesis, $Pd(acac)_2$ (0.60 mmol) and $M(acac)_x$ (0.3 mmol) (M = Ni, Zn, Sn, Ga, In, Pb) were dissolved in OLAM (40 mL). The mixture was flushed with Ar, heated quickly to 60 °C, and stirred for 30 min. After the addition of TOP (2 mL, 4.5 mmol), the mixture was heated to 200 °C (heating rate: 8 °C min^{-1}) and held for another 30 min with stirring. Afterwards, the temperature was further increased to

300 °C (heating rate: 8 °C min^{-1}) and held at 300 °C for an additional 30 min. After cooling to RT, the bimetallic PdM NCs were precipitated by the addition of ethanol and purified thoroughly by redispersion ($CHCl_3$), precipitation (ethanol), and centrifugation. Similarly, Pd NCs were prepared from $Pd(acac)_2$ (0.90 mmol) dissolved in OLAM (40 mL). After the addition of TOP (2 mL) at 60 °C (30 min), the mixture was heated to 200 °C (heating rate: 9 °C min^{-1}) and held for 30 min. After cooling to RT, the Pd NCs were purified (see above).

Preparation of catalysts: TiO_2 (P25, Evonik; 10 g) was pretreated with H_2SO_4 (2 wt%, 100 mL) for 3 h at RT with stirring. It was filtered, washed with H_2SO_4 (2 wt%), dried overnight in vacuum, and collected after grinding to powder. Metal NCs were adsorbed on the pretreated support (s-TiO_2) from the colloidal dispersion by adding s-TiO_2 (400 mg) to the appropriate amount of metal NCs in chloroform and stirring for 3 h. For most catalysts, a colorless supernatant indicated complete NC adsorption. In some cases, if some of the NCs remained dispersed in the colloidal solution (indicated by a black supernatant), ethanol (3 mL) was added, and the mixture was stirred for another 3 h. The catalysts were recovered by centrifugation, and washed with chloroform and ethanol. The final catalysts were dried (30 °C, 3 h) and ground to a fine powder.

Characterization: The NCs were analyzed by using TEM (FEI Tecnai F20 ST TEM, operated at an accelerating voltage of 200 kV, and FEI Titan 80–300, operated at an accelerating voltage 300 kV) both equipped with an EDAX EDS X-ray spectrometer (Si (Li) detecting unit, super ultra-thin window, active area 30 mm^2, resolution 135 eV at 5.9 keV). For TEM analysis, a small droplet of the colloidal NC dispersion in chloroform or the catalyst powder, accordingly, was deposited on amorphous carbon-coated 400 mesh Cu grids and dried in air. The mean particle diameter was calculated from the TEM images by measuring the size of at least 100 particles. Elemental mapping was performed by using STEM-EDX spectroscopy, and the maps were composed by integrating the corresponding elemental characteristic signal for each scanned pixel. Powder XRD patterns were recorded by using a PANalytical X'Pert Pro X-ray diffractometer employing Bragg–Brentano geometry with CuK_α radiation and a Ni filter. The Pd and M content of the dried NC powder and the supported catalysts were determined by using ICP-OES (Agilent 725 ICP-OES Spectrometer). Aqua regia and HF/aqua regia (2:1) were used to dissolve the NC powder and the catalysts for ICP-OES analysis, respectively. XAS measurements at the Pd K absorption edge were performed at the P64 beamline of the PETRA III synchrotron (DESY, Hamburg, Germany) using a QEXAFS monochromator with a channel-cut Si(111) crystal and gridded ionization chambers developed by BU Wuppertal (for details of XAS analysis, see SI).[52] Prior to XAS measurements samples were pretreated with H_2 and flushed with He to mimic the activation procedure before catalytic tests and to clean the NC surface.

Catalytic tests: All catalytic tests were performed at 30 °C and 40 bar by using a semicontinuous batch reactor (300 mL, Teflon-inlay, mechanical blowing stirrer (Teflon), and Teflon baffles) using supported NC catalysts [1.3 mg of total metal content (Pd and M) per experiment]. Ethanol (200 mL) that contained H_2SO_4 (0.12 M) or pure ethanol (200 mL) was employed as a reaction medium. Before the reaction, the slurry catalysts were activated with 4 vol% H_2 in N_2 (250 mL_{NTP} min^{-1}, NTP: normal temperature and pressure), 30 °C, 40 bar, 1 h). The reaction gas mixture (total flow 250 mL_{NTP} min^{-1}, gas composition $H_2/O_2/N_2$ 4:20:76) was introduced, and stirring was started (1000 rpm). The H_2, O_2, and N_2 concentrations that left the reactor were analyzed online by using GC (Inficon micro GC 3000). N_2 was used as an internal standard to calculate the H_2 and O_2 concentrations. The H_2O_2 concentration [$c(H_2O_2)$] was determined with $TiOSO_4/H_2SO_4$ by using UV/Vis spectrometry (Specord S600, Analytik Jena). $X(H_2)$ and $S(H_2O_2)$ were determined after 63 min of reaction from Equations (1) and (2), respectively. Typically, all catalytic tests were performed twice and mean $S(H_2O_2)$, $X(H_2)$, and $P(H_2O_2)$ values were calculated. The mean error over all experiments was 0.7 mmol L^{-1} [$c(H_2O_2)$], 1.7% [$X(H_2)$], 3.2% [$S(H_2O_2)$], and 277 mol kg_{Pd}^{-1} h^{-1} [$P(H_2O_2)$].

$$X(H_2) = \frac{\text{Consumed } H_2 \text{ [mol]}}{\text{Inlet } H_2 \text{ [mol]}} \times 100\% \quad (1)$$

$$S(H_2O_2) = \frac{n(H_2O_2) \text{ [mol]}}{H_2 \text{ consumed [mol]}} \times 100\% \quad (2)$$

Acknowledgements

S.W. thanks the Helmholtz Research School on Energy Related Catalysis for a scholarship. We thank Adam Tywoniak for his support regarding NC synthesis. We acknowledge DESY (Hamburg, Germany), a member of the Helmholtz Association HGF, for the provision of experimental facilities. Parts of this research were carried out at PETRA III, and we would like to thank Dr. Vadim Murzin (BU Wuppertal), Dr. Benjamin Bornmann (BU Wuppertal), and Dr. Wolfgang Caliebe (DESY) for assistance in using beamline P64. We would also like to acknowledge Georgios Uzunidis (KIT) for help during XAS measurements.

Conflict of interest

The authors declare no conflict of interest.

Keywords: alloys · doping · hydrogenation · nanoparticles · palladium

[1] J. M. Campos-Martin, G. Blanco-Brieva, J. L. Fierro, *Angew. Chem. Int. Ed.* **2006**, *45*, 6962 – 6984; *Angew. Chem.* **2006**, *118*, 7116 – 7139.
[2] N. M. Wilson, D. T. Bregante, P. Priyadarshini, D. W. Flaherty, *Catalysis* **2017**, *29*, 122 – 212.
[3] H. W. Kim, M. B. Ross, N. Kornienko, L. Zhang, J. Guo, P. Yang, B. D. McCloskey, *Nat. Catal.* **2018**, *1*, 282 – 290.
[4] S. Yang, A. Verdaguer-Casadevall, L. Arnarson, L. Silvioli, V. Čolić, R. Frydendal, J. Rossmeisl, I. Chorkendorff, I. E. L. Stephens, *ACS Catal.* **2018**, *8*, 4064 – 4081.
[5] a) J. S. Jirkovský, I. Panas, E. Ahlberg, M. Halasa, S. Romani, D. J. Schiffrin, *J. Am. Chem. Soc.* **2011**, *133*, 19432 – 19441; b) E. Pizzutilo, S. J. Freakley, S. Cherevko, S. Venkatesan, G. J. Hutchings, C. H. Liebscher, G. Dehm, K. J. J. Mayrhofer, *ACS Catal.* **2017**, *7*, 5699 – 5705.
[6] A. Verdaguer-Casadevall, D. Deiana, M. Karamad, S. Siahrostami, P. Malacrida, T. W. Hansen, J. Rossmeisl, I. Chorkendorff, I. E. L. Stephens, *Nano Lett.* **2014**, *14*, 1603 – 1608.
[7] S. Siahrostami, A. Verdaguer-Casadevall, M. Karamad, D. Deiana, P. Malacrida, B. Wickman, M. Escudero-Escribano, E. A. Paoli, R. Frydendal, T. W. Hansen, I. Chorkendorff, I. E. L. Stephens, J. Rossmeisl, *Nat. Mater.* **2013**, *12*, 1137 – 1143.
[8] a) Z. Lu, G. Chen, S. Siahrostami, Z. Chen, K. Liu, J. Xie, L. Liao, T. Wu, D. Lin, Y. Liu, T. F. Jaramillo, J. K. Nørskov, Y. Cui, *Nat. Catal.* **2018**, *1*, 156 – 162; b) L. Han, Y. Sun, S. Li, C. Cheng, C. E. Halbig, P. Feicht, J. L. Hübner, P. Strasser, S. Eigler, *ACS Catal.* **2019**, *9*, 1283 – 1288; c) M. Melchionna, P. Fornasiero, M. Prato, *Adv. Mater.* **2019**, *31*, 1802920.
[9] C. Xia, Y. Xia, P. Zhu, L. Fan, H. Wang, *Science* **2019**, *366*, 226 – 231.
[10] S. Fukuzumi, Y. Yamada, *ChemElectroChem* **2016**, *3*, 1978 – 1989.

[11] K. Mase, M. Yoneda, Y. Yamada, S. Fukuzumi, *Nat. Commun.* **2016**, *7*, 11470.
[12] S. J. Freakley, Q. He, J. H. Harrhy, L. Lu, D. A. Crole, D. J. Morgan, E. N. Ntainjua, J. K. Edwards, A. F. Carley, A. Y. Borisevich, *Science* **2016**, *351*, 965 – 968.
[13] S. J. Freakley, S. Kochius, J. van Marwijk, C. Fenner, R. J. Lewis, K. Baldenius, S. S. Marais, D. J. Opperman, S. T. L. Harrison, M. Alcalde, M. S. Smit, G. J. Hutchings, *Nat. Commun.* **2019**, *10*, 4178.
[14] a) R. Dittmeyer, J.-D. Grunwaldt, A. Pashkova, *Catal. Today* **2015**, *248*, 149 – 159; b) H. Henkel, W. Weber, Google Patents, **1914**; c) R. J. Lewis, G. J. Hutchings, *ChemCatChem* **2019**, *11*, 298 – 308; d) D. W. Flaherty, *ACS Catal.* **2018**, *8*, 1520 – 1527.
[15] a) Q. Liu, J. H. Lunsford, *J. Catal.* **2006**, *239*, 237 – 243; b) N. M. Wilson, D. W. Flaherty, *J. Am. Chem. Soc.* **2016**, *138*, 574 – 586; c) E. J. Lim, Y. Kim, S. M. Choi, S. Lee, Y. Noh, W. B. Kim, *J. Mater. Chem. A* **2015**, *3*, 5491 – 5500.
[16] a) Y.-F. Han, J. H. Lunsford, *J. Catal.* **2005**, *230*, 313 – 316; b) G. Gallina, J. García-Serna, T. O. Salmi, P. Canu, P. Biasi, *Ind. Eng. Chem. Res.* **2017**, *56*, 13367 – 13378; c) N. M. Wilson, D. W. Flaherty, *J. Am. Chem. Soc.* **2016**, *138*, 574 – 586.
[17] P. Tian, L. Ouyang, X. Xu, C. Ao, X. Xu, R. Si, X. Shen, M. Lin, J. Xu, Y.-F. Han, *J. Catal.* **2017**, *349*, 30 – 40.
[18] a) H. E. Jeong, S. Kim, M.-G. Seo, D.-W. Lee, K.-Y. Lee, *J. Mol. Catal. A* **2016**, *420*, 88 – 95; b) S. Kim, D.-W. Lee, K.-Y. Lee, *J. Mol. Catal. A* **2014**, *383 – 384*, 64 – 69; c) M.-G. Seo, H. J. Kim, S. S. Han, K.-Y. Lee, *Catal. Surv. Asia* **2017**, *21*, 1 – 12.
[19] G. M. Lari, B. Puertolas, M. Shahrokhi, N. Lopez, J. Perez-Ramirez, *Angew. Chem. Int. Ed.* **2017**, *56*, 1775 – 1779; *Angew. Chem.* **2017**, *129*, 1801 – 1805.
[20] a) J. K. Edwards, B. Solsona, E. Ntainjua, A. F. Carley, A. A. Herzing, C. J. Kiely, G. J. Hutchings, *Science* **2009**, *323*, 1037 – 1041; b) E. Ntainjua N, J. K. Edwards, A. F. Carley, J. A. Lopez-Sanchez, J. A. Moulijn, A. A. Herzing, C. J. Kiely, G. J. Hutchings, *Green Chem.* **2008**, *10*, 1162 – 1169; c) R. J. Lewis, J. K. Edwards, S. J. Freakley, G. J. Hutchings, *Ind. Eng. Chem. Res.* **2017**, *56*, 13287 – 13293.
[21] J. K. Edwards, S. J. Freakley, A. F. Carley, C. J. Kiely, G. J. Hutchings, *Acc. Chem. Res.* **2014**, *47*, 845 – 854.
[22] N. M. Wilson, Y.-T. Pan, Y.-T. Shao, J.-M. Zuo, H. Yang, D. W. Flaherty, *ACS Catal.* **2018**, *8*, 2880 – 2889.
[23] D. Ding, X. Xu, P. Tian, X. Liu, J. Xu, Y.-F. Han, *Chin. J. Catal.* **2018**, *39*, 673 – 681.
[24] P. Tian, X. Xu, C. Ao, D. Ding, W. Li, R. Si, W. Tu, J. Xu, Y. F. Han, *ChemSusChem* **2017**, *10*, 3342 – 3346.
[25] P. Strasser, S. Koh, T. Anniyev, J. Greeley, K. More, C. Yu, Z. Liu, S. Kaya, D. Nordlund, H. Ogasawara, M. F. Toney, A. Nilsson, *Nat. Chem.* **2010**, *2*, 454 – 460.
[26] a) Z. Niu, Y. Li, *Chem. Mater.* **2014**, *26*, 72 – 83; b) P. Liu, R. Qin, G. Fu, N. Zheng, *J. Am. Chem. Soc.* **2017**, *139*, 2122 – 2131.
[27] a) M. Cargnello, V. V. T. Doan-Nguyen, C. B. Murray, *AIChE J.* **2016**, *62*, 392 – 398; b) M. Cargnello, V. V. T. Doan-Nguyen, T. R. Gordon, R. E. Diaz, E. A. Stach, R. J. Gorte, P. Fornasiero, C. B. Murray, *Science* **2013**, *341*, 771 – 773; c) S.-W. Kim, J. Park, Y. Jang, Y. Chung, S. Hwang, T. Hyeon, Y. W. Kim, *Nano Lett.* **2003**, *3*, 1289 – 1291; d) S. G. Kwon, T. Hyeon, *Acc. Chem. Res.* **2008**, *41*, 1696 – 1709.
[28] C. Amatore, A. Jutand, M. A. M'Barki, *Organometallics* **1992**, *11*, 3009 – 3013.
[29] J. J. Willis, E. D. Goodman, L. Wu, A. R. Riscoe, P. Martins, C. J. Tassone, M. Cargnello, *J. Am. Chem. Soc.* **2017**, *139*, 11989 – 11997.
[30] Z. Luo, J. Lu, C. Flox, R. Nafria, A. Genç, J. Arbiol, J. Llorca, M. Ibáñez, J. R. Morante, A. Cabot, *J. Mater. Chem. A* **2016**, *4*, 16706 – 16713.
[31] a) A. Santos, R. J. Lewis, G. Malta, A. G. R. Howe, D. J. Morgan, E. Hampton, P. Gaskin, G. J. Hutchings, *Ind. Eng. Chem. Res.* **2019**, *58*, 12623 – 12631; b) F. Li, Q. Shao, M. Hu, Y. Chen, X. Huang, *ACS Catal.* **2018**, *8*, 3418 – 3423.
[32] B. E. Solsona, J. K. Edwards, P. Landon, A. F. Carley, A. Herzing, C. J. Kiely, G. J. Hutchings, *Chem. Mater.* **2006**, *18*, 2689 – 2695.
[33] a) Y.-F. Han, Z. Zhong, K. Ramesh, F. Chen, L. Chen, T. White, Q. Tay, S. N. Yaakub, Z. Wang, *J. Phys. Chem. C* **2007**, *111*, 8410 – 8413; b) N. M. Wilson, J. Schröder, P. Priyadarshini, D. T. Bregante, S. Kunz, D. W. Flaherty, *J. Catal.* **2018**, *368*, 261 – 274.
[34] G. Bernardotto, F. Menegazzo, F. Pinna, M. Signoretto, G. Cruciani, G. Strukul, *Appl. Catal. A* **2009**, *358*, 129 – 135.
[35] a) G. Li, J. Edwards, A. F. Carley, G. J. Hutchings, *Catal. Today* **2006**, *114*, 369 – 371; b) I. Chorkendorff, J. W. Niemantsverdriet, *Concepts of Modern Catalysis and Kinetics*, Wiley-VCH, Weinheim, **2017**; c) R. J. Lewis, K. Ueura, Y. Fukuta, S. J. Freakley, L. Kang, R. Wang, Q. He, J. K. Edwards, D. J. Morgan, Y. Yamamoto, G. J. Hutchings, *ChemCatChem* **2019**, *11*, 1673 – 1680.
[36] F. Alotaibi, S. Al-Mayman, M. Alotaibi, J. K. Edwards, R. J. Lewis, R. Alotaibi, G. J. Hutchings, *Catal. Lett.* **2019**, *149*, 998 – 1006.
[37] S. Lee, Y.-M. Chung, *Mater. Lett.* **2019**, *234*, 58 – 61.
[38] J. K. Edwards, S. J. Freakley, R. J. Lewis, J. C. Pritchard, G. J. Hutchings, *Catal. Today* **2015**, *248*, 3 – 9.
[39] a) P. Centomo, C. Meneghini, S. Sterchele, A. Trapananti, G. Aquilanti, M. Zecca, *ChemCatChem* **2015**, *7*, 3712 – 3718; b) M. Selinsek, B. J. Deschner, D. E. Doronkin, T. L. Sheppard, J.-D. Grunwaldt, R. Dittmeyer, *ACS Catal.* **2018**, *8*, 2546 – 2557.
[40] S. J. Freakley, M. Piccinini, J. K. Edwards, E. N. Ntainjua, J. A. Moulijn, G. J. Hutchings, *ACS Catal.* **2013**, *3*, 487 – 501.
[41] a) A. Egeberg, C. Dietrich, C. Kind, R. Popescu, D. Gerthsen, S. Behrens, C. Feldmann, *ChemCatChem* **2017**, *9*, 3534 – 3543; b) W. Liu, Y. Chen, H. Qi, L. Zhang, W. Yan, X. Liu, X. Yang, S. Miao, W. Wang, C. Liu, A. Wang, J. Li, T. Zhang, *Angew. Chem. Int. Ed.* **2018**, *57*, 7071 – 7075; *Angew. Chem.* **2018**, *130*, 7189 – 7193.
[42] S. Wang, R. J. Lewis, D. E. Doronkin, D. J. Morgan, J.-D. Grunwaldt, G. J. Hutchings, S. Behrens, *Catal. Sci. Technol.* **2020**, *10*, 1925 – 1932.
[43] S. Maity, M. Eswaramoorthy, *J. Mater. Chem. A* **2016**, *4*, 3233 – 3237.
[44] a) S. Furukawa, T. Komatsu, *ACS Catal.* **2017**, *7*, 735 – 765; b) Y. Yan, J. S. Du, K. D. Gilroy, D. Yang, Y. Xia, H. Zhang, *Adv. Mater.* **2017**, *29*, 1605997; c) M. Gentzen, D. E. Doronkin, T. L. Sheppard, A. Zimina, H. Li, J. Jelic, F. Studt, J.-D. Grunwaldt, J. Sauer, S. Behrens, *Angew. Chem. Int. Ed.* **2019**, *58*, 15655 – 15659; *Angew. Chem.* **2019**, *131*, 15802 – 15806; d) M. Gentzen, D. E. Doronkin, T. L. Sheppard, J.-D. Grunwaldt, J. Sauer, S. Behrens, *Appl. Catal. A* **2018**, *562*, 206 – 214.
[45] H. C. Ham, J. A. Stephens, G. S. Hwang, J. Han, S. W. Nam, T. H. Lim, *Catal. Today* **2011**, *165*, 138 – 144.
[46] N. M. Wilson, P. Priyadarshini, S. Kunz, D. W. Flaherty, *J. Catal.* **2018**, *357*, 163 – 175.
[47] H. Xu, D. Cheng, Y. Gao, *ACS Catal.* **2017**, *7*, 2164 – 2170.
[48] C. Dietrich, D. Schild, W. Wang, C. Kübel, S. Behrens, *Z. Anorg. Allg. Chem.* **2017**, *643*, 120 – 129.
[49] a) J. K. Edwards, A. Thomas, A. F. Carley, A. A. Herzing, C. J. Kiely, G. J. Hutchings, *Green Chem.* **2008**, *10*, 388 – 394; b) J. K. Edwards, E. Ntainjua N, A. F. Carley, A. A. Herzing, C. J. Kiely, G. J. Hutchings, *Angew. Chem. Int. Ed.* **2009**, *48*, 8512 – 8515; *Angew. Chem.* **2009**, *121*, 8664 – 8667.
[50] S. Wang, K. Gao, W. Li, J. Zhang, *Appl. Catal. A* **2017**, *531*, 89 – 95.
[51] T. Bligaard, R. M. Bullock, C. T. Campbell, J. G. Chen, B. C. Gates, R. J. Gorte, C. W. Jones, W. D. Jones, J. R. Kitchin, S. L. Scott, *ACS Catal.* **2016**, *6*, 2590 – 2602.
[52] O. Müller, D. Lützenkirchen-Hecht, R. Frahm, *Rev. Sci. Instrum.* **2015**, *86*, 093905.

Manuscript received: February 14, 2020
Revised manuscript received: March 27, 2020
Accepted manuscript online: March 31, 2020
Version of record online: May 11, 2020

